Microbialite response to an anthropogenic salinity gradient in Great Salt Lake, Utah

M. R. Lindsay[1], C. Anderson[2], N. Fox[2], G. Scofield[2], J. Allen[2], E. Anderson[1], L. Bueter[1], S. Poudel[1], K. Sutherland[2], J. H. Munson-McGee[1], J. D. Van Nostrand[3], J. Zhou[3,4,5], J. R. Spear[6,8], B. K. Baxter[7], D. R. Lageson[2], E. S. Boyd[1,8]

[1] Department of Microbiology and Immunology, Montana State University, Bozeman, MT, USA [2] Department of Earth Sciences, Montana State University, Bozeman, MT, USA [3] Department of Microbiology and Plant Biology, University of Oklahoma, Norman, OK, USA [4] State Key Joint Laboratory of Environment Simulation and Pollution Control, School of Environment, Tsinghua University, Beijing, China [5] Earth Science Division, Lawrence Berkeley National Laboratory, Berkeley, CA, USA [6] Department of Civil and Environmental Engineering, Colorado School of Mines, Golden, CO, USA [7] Department of Biology, Westminster College, Salt Lake City, UT, USA [8] NASA Astrobiology Institute, Mountain View, CA, USA

Correspondence E. S. Boyd, Department of Microbiology and Immunology, Montana State University, Bozeman, MT, USA. Email: eboyd@montana.edu

Abstract

A railroad causeway across Great Salt Lake, Utah (GSL), has restricted water flow since its construction in 1959, resulting in a more saline North Arm (NA; 24%–31% salinity) and a less saline South Arm (SA; 11%–14% salinity). Here, we characterized microbial carbonates collected from the SA and the NA to evaluate the effect of increased salinity on community composition and abundance and to determine whether the communities present in the NA are still actively precipitating carbonate or if they are remnant features from prior to causeway construction. SSU rRNA gene abundances associated with the NA microbialite were three orders of magnitude lower than those associated with the SA microbialite, indicating that the latter community is more productive. SSU rRNA gene sequencing and functional gene microarray analyses indicated that SA and NA microbialite communities are distinct. In particular, abundant sequences affiliated with photoautotrophic taxa including cyanobacteria and diatoms that may drive carbonate precipitation and thus still actively form microbialites were identified in the SA microbialite; sequences affiliated with photoautotrophic taxa were in low abundance in the NA microbialite. SA and NA microbialites comprise smooth prismatic aragonite crystals. However, the SA microbialite also contained micritic aragonite, which can be formed as a result of biological activity. Collectively, these observations suggest that NA microbialites are likely to be remnant features from prior to causeway construction and indicate a strong decrease in the ability of NA microbialite communities to actively precipitate carbonate minerals. Moreover, the results suggest a role for cyanobacteria and diatoms in carbonate precipitation and microbialite formation in the SA of GSL.

1 Introduction

The oldest identifiable fossil assemblages and evidence of life from Earth's early biosphere (3.481 Ga) are putative microbialites (Allwood, Walter, Kamber, Marshall, & Burch, 2006; Sugitani et al., 2015; Van Kranendonk, Philippot, Lepot, Bodorkos, & Pirajno, 2008; Walter, Buick, & Dunlop, 1980). Interactions between microbial communities and their environments in modern settings can result in the formation of organo-sedimentary structures, termed microbialites. Modern microbialites often display microstructures similar to those identified in Precambrian rocks which, along with other evidence, have led to the interpretation of the latter structures as being biogenic (Laval et al., 2000). Studies on modern microbialites can provide insights into how biological communities and processes influence the formation and preservation of microbialite fabrics (Baumgartner et al., 2009; Bosak, Knoll, & Petroff, 2013; Jahnert & Collins, 2011; Pepe-Ranney, Berelson, Corsetti, Treants, & Spear, 2012; Reid et al., 2000). Moreover, such studies can inform our understanding of the physiology and ecology of this early life and its potential role in ecosystem primary production during that time (Edgcomb et al., 2014).

Microbialites are subdivided into five specific types: stromatolites, thrombolites, dendrolites, leiolites, and microbially induced sedimentary structures (MISS) (Noffke & Awramik, 2013; Riding, 2000). With the exception of MISS, which form with little or no carbonate or mineral precipitation (Noffke & Awramik, 2013), the most important process in the formation of microbialite structures is carbonate precipitation driven by localized increases in alkalinity. The increase in alkalinity is induced by the consumption of carbon dioxide or bicarbonate through metabolic processes such as autotrophic photosynthesis, ammonification, denitrification, and sulfate reduction, among others (Riding, 2011). The most common metabolic process resulting in microbialite formation in modern environments is autotrophic photosynthesis carried out by cyanobacteria or algae (Dupraz & Visscher, 2005; Riding, 2000). Sediment trapping and binding by microbial extracellular polymeric substances (Gebelein, 1969) also play key roles in the formation of microbialite structures (Dupraz et al., 2009; Riding, 2000).

Prior to the Cambrian explosion ~542 Ma, microbialites were likely widespread in shallow marine seas (Riding, 2000) and on the edges of freshwater lakes (Osborne, Licari, & Link, 1982). Today, microbialites can still be found in saline marine environments such as in the Hamelin Pool of Shark Bay, Western Australia (Collins & Jahnert, 2014; Logan, 1961; Pages et al., 2014), and in Highborne Cay, Bahamas (Myshrall et al., 2010). These structures are also found in modern lacustrine environments including Pavilion Lake, Canada (Laval et al., 2000), Lake Tanyangika, Africa (Cohen, Talbot, Awramik, Dettman, & Abell, 1997), Lake Salda Golu, Turkey (Braithwaite & Zedef, 1994), Cuatro Cienegas, Mexico (Souza et al., 2006), Lake Alchichica, Mexico (Gerard et al., 2013), Ruidera Pools, Spain (Foster &

Green, 2011), and Great Salt Lake (GSL), United States (Chidsey, Vanden Berg, & Eby, 2015; Roney, Booth, & Cox, 2009).

Great Salt Lake is the largest lake in the western United States and the fourth largest terminal lake in the world (52,000 km^2) (Hassibe & Keck, 1991). GSL is a shallow, meromictic lake that exhibits a maximum and a mean depth of ~9.0 and 4.3 m, respectively. Microbialites and their associated microbial communities are extensive in GSL due to the hypersaline conditions, as well as the shallow nature of the lake (Fig. 1B) (Colman, Kelts, & Dinter, 2002; Wurtsbaugh, 2009). In particular, extensive shallow margins are conducive to sunlight penetration throughout the water column, promoting growth of photoautotrophic micro-organisms which in turn are thought to drive the formation of the microbialites (Chidsey et al., 2015). Much of the sediment that provides a base for microbialites in GSL is oolitic sand, which are small spherical to elongated grains composed of radial aragonite crystalline fabrics surrounding a core of either detrital mineral grains or brine shrimp fecal pellets (Chidsey et al., 2015; Eardley, 1938; Gwynn, 1996). Microbialite structures in GSL grow on lithified crusts of oolitic sands and lime muds, often resulting in substantial microbialite reef-like complexes (Riding, 2000).

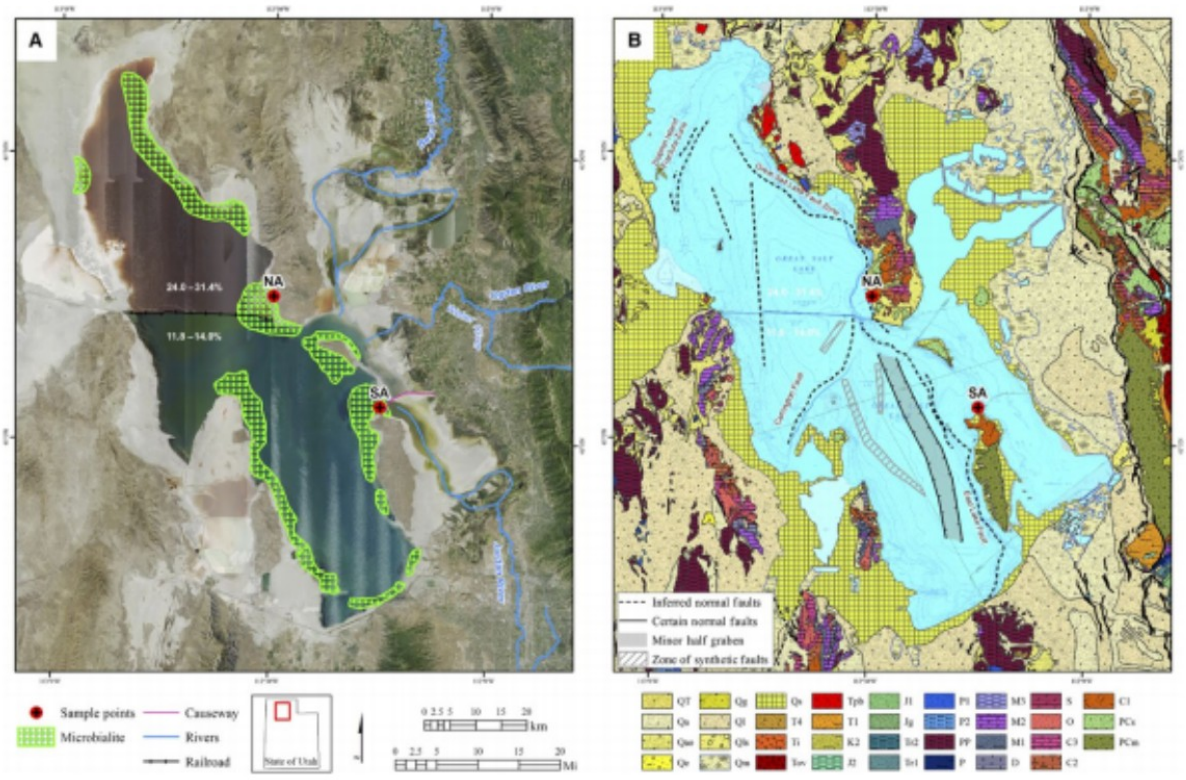

FIGURE 1 A) Map of the GSL constructed with salinity (%), structural, stream, transportation, and microbialite reference layers. Imagery from NAIP 1 m resolution orthoimagery (2014) accessed from Utah Geological Survey (UGS) server. Salinity values for South Arm (SA) and North Arm (NA) were

determined as part of this study and known ranges included from Chidsey et al., 2015;. Microbialite layer modified from Eardley (1938) (Eardley, 1938). Stream data modified from National Hydrological Dataset (USGS, EPA, State of Utah). Railroad layer digitized from 1 m NAIP Imagery (2014). B) Geologic and bathymetric map of GSL. Data layers: Geology from Utah Geologic Survey (1:500,000). Structure: Colman et al., 2002 (Colman et al., 2002) and UGS Quaternary Fault and Fold Database (2013). Geologic unit descriptions: Q: Quaternary QT: high-level alluvial deposits, Qa: surficial alluvium and colluvium, Qao: surficial older alluvium and colluvium, Qe: surficial eolian deposits, surficial glacial deposits, Ql: surficial Lake Bonneville deposits, Qls: surficial landslide deposits, Qm: surficial marsh deposits, Qs: surficial mud and salt flat deposits, T: Tertiary, T4: Salt Lake Fm and other valley-filling alluvial, lacustrine, and volcanic units, Ti: intrusive rocks, Tov: volcanic rocks, Tpb: volcanic rocks—mostly basalt, K: Cretaceous, K2: Indianola, Mancos, Frontier, Straight Cuffs, Iron Springs, and other Formations, T1: Wasatch, Cotton, Flagstaff, Claron, White Sage, and other Formations, J: Jurassic, J2: Morrison Formation, J1: Summerville, Entrada, Carmel, Arapien, Twin Creek, and other Formations, Jg: Glen Canyon Group (Navajo, Kayenta, Wingate, Moenave Fms) and Nugget Ss, Tr: Triassic, Tr2: Chinle and Ankareh Formations, Tr1: Moenkopi, Dinwoody, Woodside, Thaynes, and other Formations, P: Permian, P1: Cedar Mesa, Diamond Creek, Arcturus, and other Formations, P2: Kaibab, Toroweap, Park City, and other Formations, PP: Pennsylvanian-Permian Oquirrh Group, Wells, Weber, Ely, Callville, and other Formations, P: Permian Morgan, Round Valley, Pennsylvanian Honaker Trail, Paradox, Ely, and other Formations, M: Mississippian, M3: Chainman, Manning Canyon, Doughnut, and other Formations, M2: Great Blue, Humbug, Deseret, and other Formations, M1: Redwall, Madison, Gardison, Ludgepole, and other Formations, D: Devonian Formations, S: Silurian Laketown and Bluebell Dolomite, O: Ordovician Fish Haven, Swan Peak, Garden City, Eureka, and other Formations, C: Cambrian, C3: St. Charles, Nounan, Bloomington, and other Upper Cambrian Formations, C2: Middle Cambrian Formations, C1: Prospect Mountain, Tintic, Ignacio, Geertsen Canyon, and other Formations, PCs: Proterozoic sedimentary and metasedimentary formations, PCm: Precambrian metamorphic rocks; Structure: (Colman et al., 2002), and UGS Quaternary Fault and Fold Database (2013). Bathymetry modified from (Baskin & Allen, 2005; Baskin & Turner, 2006)

The construction of a rock and gravel railroad causeway in 1959 segregated GSL into a North Arm (NA) and South Arm (SA), and the restricted flow of water between these two ‘arms’ created an artificial salinity gradient (Cannon & Cannon, 2002). Seven years after construction of the causeway, Greer (2002) sampled the brine composition of the NA and SA during low lake datum and found that they were 27.3% and 20.6% saline, respectively (Greer 1971). Thirty years later, the salinities of the NA and the SA diverged to >24% and 12%–14%, respectively (Chidsey et al., 2015; Gwynn, 1996). The NA salinity is typically at saturation [~5 M, 270–300 g L^{-1} total dissolved solids (TDS)] (Baxter et al., 2005), whereas salinity in the SA surface brine is substantially lower (~ 2.5 M, 140–150 g L^{-1} TDS) due to freshwater inputs from three rivers (Jordan, Bear, and Weber rivers). Salinity gradients in the lake have been shown to markedly influence the structure and composition of planktonic microbial communities (Boyd et al., 2014; Meuser et al., 2013; Parnell et al., 2010). However, little is known about the influence of salinity on the composition of communities that are associated with GSL microbialite structures although the macroscopic morphology and mineralogy of the structures themselves are well characterized (Chidsey et al., 2015; Eardley, 1938; Halley, 1976; Pedone & Folk, 1996).

To date, the most substantive characterization of microbial communities associated with GSL carbonate structures (e.g., microbialites) was performed by Post (1977). Based on cultivation and microscopic analysis, the carbonate structure-associated communities consisted mainly of the archaeal taxa *Halobacterium* and *Halococcus,* the algal taxa *Dunaliella salina* and *Dunaliella viridis*, and the invertebrate taxa *Artemia salina, Ephydra gracilis,*

and *Ephydra hians* (Post, 1977). In addition to the characterizations by Post (1977), Halley (1976) described a cyanobacterial species that was associated with substantial sectors of SA microbialite structures in waters with salinities as high as 160 g L^{-1}. Microbialites sampled from GSL in slightly lower salinity waters (130 g L^{-1}) were reported to be comprised primarily of diatoms (Collins, 1980). A more recent analysis of microbialites sampled from the SA also indicated the presence of abundant chlorophyll, suggesting a role for phototrophs in the formation of the microbialites (Wurtsbaugh, Gardberg, & Izdepski, 2011). Moreover, observations of a nearly uniform morphotype, which is thought to be affiliated with the cyanobacterial genus *Aphanothece*, in association with SA carbonate structures at the time of the sample collection support this prediction (Wurtsbaugh et al., 2011).

In this study, we hypothesized that the construction of the railroad causeway in 1959 and the hypersaline conditions that developed significantly impacted the composition and structure of NA microbialite communities. Considering that the carbon dioxide consuming activity of phototrophs, the most likely culprits for carbonate precipitation and microbialite formation in GSL, is highly sensitive to salinity stress (Joint, Henriksen, Garde, & Riemann, 2002), we also hypothesized that carbonate precipitation in the NA is no longer occurring biogenically. To investigate these interrelated hypotheses, we characterized the abundance of SSU rRNA gene templates, SSU rRNA and functional gene diversity, mineralogy, and morphology of microbialites sampled from the saline SA of the GSL near Antelope Island. Molecular and morphological analyses conducted on a SA microbialite were compared to a complementary dataset collected on a microbialite sampled from the hypersaline NA of GSL near Little Valley Marina. In addition, molecular data were collected on planktonic communities sampled adjacent to microbialites from both the SA and NA. The combined mineralogical, morphological, and molecular characterization of GSL microbialites provides new constraints on the populations and processes likely involved in the formation of such structures under vastly different conditions of water chemistry. Our observations provide new insights into the formation of GSL microbialites and inform our understanding of the processes that may have been involved in the formation of similar structures present in the geologic record.

2 Materials and methods

2.1 Geologic setting

GSL occupies one of the lowest depressions in the Great Basin Province bounded by the north–south trending Wasatch fault zone to the east (Baskin, 2014; Chidsey et al., 2015; Cohenour & Thompson, 1966). During the Cretaceous, the Sevier orogenic system produced thrust faults and folds across the region that would become the GSL basin (Mohapatra & Johnson, 1998). From the middle Eocene to early Miocene (49–20 Ma), crustal extension caused collapse, and a subsequent stage of extension produced

the current Basin and Range structural architecture from middle Miocene to the present (17 Ma - present) (Mohapatra & Johnson, 1998).

The basin occupied by GSL is a half graben produced by extensional faults, and the older bedrock beneath GSL experiences multiple phases of brittle deformation and is highly fractured (Baskin, 2014; Cohenour & Thompson, 1966; Gwynn, 1996; Jones, Naftz, Spencer, & Oviatt, 2009; Mohapatra & Johnson, 1998). Other than the most extensive Northern Hemisphere glaciations which formed the larger Lake Bonneville, the current GSL area (Fig. 1A,B) and its characteristics are likely similar to what they have been the last 780 ka (Oviatt, Madsen, Miller, Thompson, & Mcgeehin, 2015; Oviatt, Thompson, Kaufman, Bright, & Forester, 1999) or even longer (Charles Oviatt, *pers. comm*). The major source of freshwater inflow to GSL comes from three major rivers (the Bear, Weber, and Jordan Rivers), all of which flow into the SA (Baskin, 2014; Chidsey et al., 2015; Gwynn, 1996; Jones et al., 2009; Naftz, Millero, Jones, & Green, 2011; Tazi, Breakwell, Harker, & Crandall, 2014). This results in fluctuating salinity in the SA, while salinity in the NA is maintained at near the saturation of sodium chloride (Gwynn, 1996; Naftz et al., 2011). While the abundance of ions is higher in the NA than the SA, the composition of ions is similar between these two areas (Domagalski, Orem, & Eugster, 1989). Adding to the effects of salinity, mirabilite deposits on the lake bottom or in the subsurface from past extreme drought conditions contribute to salinity and nutrient supply to GSL (Anderson et al., 2014; Oviatt et al., 2015), perhaps influenced by the faults cross-cutting the lake bottom (Fig. 1A) (Velasco, Bennett, Johnson, & Hreinsdóttir, 2010).

2.2 Description of sample sites and associated microbialites

The microbialites in GSL were first mapped and described in detail by Eardley (Eardley, 1938) during the droughts of 1933 and 1934 (Fig. 1A) with the microbialite expanse quantified to 100 mi^2. Morphologies of GSL microbialites were described by Carozzi (1962) from observations offshore Promontory Point and categorized from lake to shoreline into four zones: (i) subparallel festooned ridges, (ii) tongue-like festooned ridges, (iii) composite rings and flat-topped mounds, and (iv) isolated mounds (Carozzi, 1962). After making cross sections of these zones, Carozzi (1962) found that they were merely the exaggerated expression of underlying topography carved from argillaceous and oolitic sediments. Similarly, Chidsey et al. (2015) also found microbialite mounds shaped as domal stromatolites at Bridger Bay on the northwestern tip of Antelope Island (Chidsey et al., 2015). Like the microbialites sampled in this study (described below), those sampled by Chidsey were low-profile domical structures with some structures exhibiting a raised outer ring morphology (Fig. 2A). Their shape was created by wave erosion of ooid and argillaceous sand from around the base of the microbialite mound. The microstructure of microbialites was found to be mixed laminated or lacking lamination (Halley, 1976).

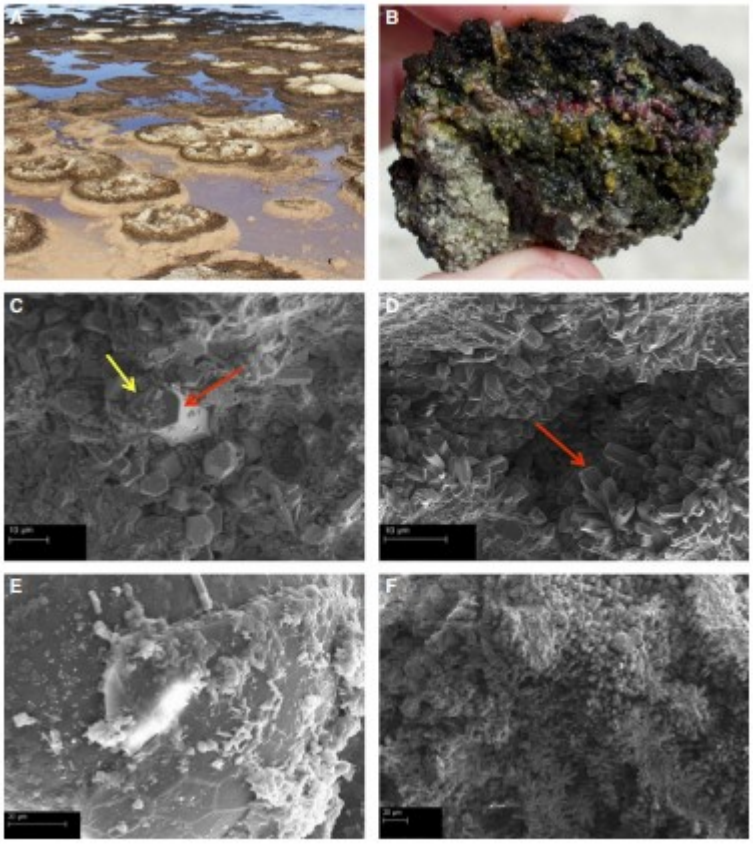

FIGURE 2 A) South Arm (SA) microbialites. Image taken on November 10, 2015. Rings in the microbialites are the result of decreasing water levels within the lake (Vanden Berg, Chidsey, Eby, & Kelln, 2015). Mud and ooids within the microbialites compact as the water table drops and the microbialite structure collapses. The upper white portion of the microbialite structure is a result of bleaching (Chidsey et al., 2015). B) Cross-sectional image of SA microbialite hand sample, with layers of biomass on top of hardened gray carbonate. C) FEM image of SA orthorhombic aragonite crystals (indicated by the red arrow) overlain with micritic aragonite precipitates (yellow arrow). D) FEM image of a pore space in a North Arm (NA) microbialite that is filled with crystalline aragonite (indicated by the red arrow) lacking micritic aragonite precipitates. E) FEM image of a SA microbialite-associated *Artemia* (brine shrimp) cyst at 2600×. F) FEM image of NA microbialite showing an abundance of crystalline aragonite

Recent mapping of the faults in the Great Salt Basin, coupled with the microbialite distribution maps of Eardley (1938) and others, suggests that the underlying structural geology likely plays a key role in defining the distribution of the microbialites in GSL (Fig. 1A) (Eardley, 1938). High-resolution seismic reflection data indicate that the distribution of microbialites is directly associated with microtopographic highs that result from faults, folds, or monoclinal features on the floor of GSL (Baskin, Driscoll, & Wright, 2013; Baskin, Wright, Driscoll, Kent, & Hepner, 2012). One of the key faults that appears to directly affect microbialite distribution is the East Lake Fault which defines the eastern and southeastern margin of GSL (Bouton et al., 2016). Oil seeps and their associated brine solutions found along the north–northeast margin of GSL may be contributing nutrients to the lake bottom which could be utilized by microbialite populations (Sei & Fathepure, 2009). This spatial correspondence suggests that seepage of

basinal fluids upwards along fault surfaces beneath microbialite structures may provide minerals and nutrients that facilitate the growth of microbialites (Baskin et al., 2012, 2013; Colman et al., 2002).

2.3 Sample collection

Microbialite samples and samples of planktonic cells in adjacent waters were collected in July of 2011. Samples from the NA were collected just offshore from Little Valley Harbor (N 41.2557, W −112.4991). Samples from the SA were collected just offshore of Antelope Island Marina (N 41.0639, W −112.2487). The NA water sample was 20°C and had a pH of 7.9 and salinity of 31.4% (as measured with a field refractometer). In contrast, the SA water sample was 18°C and had a pH of 7.2 and a salinity of 11.8%. Samples of microbialite (250 g) were collected and placed in sterile Whirl-Pak (Nasco) bags and were frozen (−20°C) until used for molecular, morphological, and mineralogical analysis. Submerged microbialites that were visually representative of the morphology of the structures in each location were collected. The samples collected in this study area are from shallow littoral areas and are affected by subtle changes in lake level and wind-driven waves similar to processes in an intertidal environment. Samples of water (2 ml) adjacent to each sampled microbialite, collected using a sterile syringe, were transferred to a 2-ml cryovial and were frozen immediately (−20°C) until used for DNA extraction.

In the laboratory, NA and SA microbialite samples were thawed overnight at 4°C and three replicate subsamples (~ 250 mg) of each microbialite were removed with a flame-sterilized chisel (NA) or spatula (SA). Subsamples were transferred to sterile bead beating tubes and stored at −20°C until used for molecular analyses. A single water column sample from the SA and the NA sampling sites was concentrated by centrifugation (14,000 × g, 15 min., 4°C) and the pellet was resuspended in 100 µl of sterile phosphate buffer provided in the FastDNA Spin Kit for Soil (MP Biomedicals). The cell suspensions were then transferred to sterile bead beating tubes and stored at −20°C until used for molecular analyses.

2.4 DNA extraction, sequencing, and analysis

DNA was extracted from each microbialite sample and from the water column samples using the FastDNA Spin Kit for Soil (MP Biomedicals). The concentration of DNA in each extract was determined using the Qubit dsDNA HS Assay kit (Molecular Probes). Replicate extracts were combined for use in PCR analysis and sequencing, but were kept separate for qPCR and functional gene microarray analysis (described below).

Genomic DNA was subjected to PCR amplification of 16S rRNA (Bacteria and Archaea) and 18S rRNA (Eukarya) genes. Thirty-five cycles of PCR were conducted using 15 ng of template DNA and bacterial-specific 16S rRNA gene primers 1100F/1492R primers (annealing temperature of 55°C), archaeal-specific 16S rRNA gene primers 344F/958R (annealing temperature

of 62°C), or eukaryl-specific 18S rRNA gene primers A7F/570R (annealing temperature of 42°C) as previously described (Hamilton, Peters, Skidmore, & Boyd, 2013). Cycling conditions included an initial denaturation step at 95°C for 5 min followed by 35 cycles of 95°C (1 min.), annealing at specified temperature (1 min.), and extension at 72°C (1.5 min.), with a final extension step at 72°C for 10 min.

Archaeal, bacterial, and eukaryl 16S/18S rRNA gene amplicons were sequenced by MrDNA (Shallowater, TX). Amplicons from each sample were barcoded as previously described (Dowd et al., 2008) using the primers described above and were sequenced using a 454 Genome Sequencer FLX System. Post-sequence processing was performed with Mothur (ver. 1.36.1) (Schloss et al., 2009) as previously described (Hamilton et al., 2013). Briefly, raw libraries were trimmed to a minimum length of 350 (Archaea), 360 (Bacteria), and 300 (Eukarya) bases and were subjected to a filtering step using the quality scores file to remove sequences with anomalous base calls. Unique sequences were aligned using domain-specific SILVA databases, and sequences were trimmed using a defined start and end site based on inclusion of 75% of the total sequences; sequences that started before or after these defined positions were removed without further consideration. The resultant unique sequences were pre-clustered to remove amplification and sequencing errors, and chimeras were identified and removed using UCHIME (Edgar, Haas, Clemente, Quince, & Knight, 2011). Operational taxonomic units (OTUs) were assigned at a sequence similarity of 0.97 using the nearest-neighbor method. The remaining sequences were randomly subsampled to normalize the total number of sequences in each library. Collectively, these steps resulted in a normalized size of 5360, 5188, and 1237 SSU rRNA gene sequences for each archaeal, bacterial, and eukaryal library, respectively. Rarefaction curves were used to compute the percent coverage of the predicted taxonomic richness for each library. Sequences were classified using the Bayesian classifier (Wang, Garrity, Tiedje, & Cole, 2007) and the RDP database, with manual verification using BLASTn. Raw reads, quality scores, and mapping files for the archaeal, bacterial, and eukaryl 16S/18S rRNA gene libraries have been deposited in the NCBI short reads archive under accession number SRR2976523.

2.5 qPCR

Quantitative PCR (qPCR) was used to estimate the number of 16S (Archaea, Bacteria) and 18S rRNA (Eukarya) gene templates associated with SA and NA microbialites. Methods for qPCR generally followed our previously described methods (Hamilton et al., 2013) and used archaeal, bacterial, and eukaryl 16S/18S rRNA gene-containing plasmids to generate standard curves. qPCR assays were performed in a Rotor-Gene 300 quantitative real-time PCR machine (Qiagen, Valencia, CA) in 0.1 ml optically clear PCR tubes (Qiagen, Valencia, CA) using a SsoFast™ EvaGreen Supermix qPCR Kit (Bio-Rad Laboratories, Hercules, CA). qPCR cycling conditions were as follows: initial denaturation (95°C for 10 min) followed by 40 cycles of denaturation (95°C

for 10 s), annealing at specified temperatures (see above), and extension (72°C for 20 s). Specificity of the qPCR assays was verified by melt curve analysis. Negative control assays were performed in the absence of template DNA. Each assay was performed in triplicate, and the reported template abundances are the average and standard deviation of triplicate determinations. Template abundances were normalized to grams dry mass (gdm) of the extracted microbialite, as determined by drying the bead beating extraction tubes at 80°C for 24 hrs. Following drying, the mass of the residue was determined after accounting for the mass of an empty extract tube and contents.

2.6 Functional gene microarray analysis

Genomic DNA was subjected to functional gene analysis using the GeoChip (vers. 5.0) microarray platform. The GeoChip is a functional gene array that contains 167,044 probes covering 395,894 coding sequences from ~1,500 gene families. Genomic DNA (1 μg) was mixed with 5.5 μl random primers (Life Technologies, random hexamers, 3 μg μl^{-1}), brought to a 35 μl volume with nuclease-free water, heated to 99°C for 5 min, and immediately placed on ice. The labeling master mix (15 μl [2.5 μl of dNTP (5 mM dAGC-TP, 2.5 mM dTTP), 0.5 μl of Cy-3 dUTP (25 nM; GE Healthcare), 1 μl of Klenow (imer; San Diego, CA; 40 U ml^{-1}), 5 μl Klenow buffer, 2.5 μl of water]) was added, and the samples were incubated at 37°C for 6 hr in a thermocycler and then at 95°C for 3 min to inactivate the enzyme. After the addition of Cy3, samples were protected from the light as much as possible. Labeled DNA was cleaned using a QIAquick purification kit (Qiagen) as per the manufacturer's instructions and then dried down in a SpeedVac (45°C, 45 min; ThermoSavant). Labeled DNA was rehydrated in 27.5 μl nuclease-free water and 99.4 μl hybridization buffer, and then, 120 μl of this hybridization mix was loaded onto the GeoChip and hybridized at 67°C for 20–22 hr as described previously (Wang et al., 2014).

2.7 Microarray scanning and data processing

GeoChips were imaged (NimbleGen MS 200 microarray scanner) as a Multi-TIFF. The data were then extracted using the Agilent Feature Extraction program. Extracted data were then loaded onto the GeoChip data analysis pipeline (ieg.ou.edu/microarray/). Data normalization and quality filtering were performed with multiple steps (Liang et al., 2010). First, the average signal intensity of the common oligo reference standard was calculated for each array, and the maximum average value was applied to normalize the signal intensity of samples in each array. Second, the sum of the signal intensity of samples was calculated for each array, and the maximum sum value was applied to normalize the signal intensity of all spots in an array, which produced a normalized value for each spot in each array. Spots were scored as positive based on a floating signal-to-noise ratio [SNR = (signal mean—background mean)/background standard deviation] so that hyperthermophile control probes accounted for 2% of positive probes. In

addition, spots with background coefficients of variation (CV) <0.8 were removed.

To simplify downstream analyses, processed GeoChip data were subjected to a filtering step whereby all probes with an average threshold intensity of less than 0.8 were removed from the dataset without further consideration. Secondarily, probes that did not yield a signal in two of the three replicates (i.e., singlets) were discarded without further consideration. A custom python script was used to identify the unique probes (i.e., genes) detected in the SA and NA and to identify probes that were present in both samples.

Principle component analysis (PCA) was applied to the filtered GeoChip data to visualize variation in the samples. PCA analysis was computed using the correlation matrix generated using the hybridization intensity matrix with FactoMineR package in R (Le, Josse, & Husson, 2008). PCA analysis of the GeoChip data revealed that replicate SA and NA microbialite genomic DNA formed two clusters along PCA axis 1. Thus, a custom python script was written to identify probes that contributed to the pattern of clustering along this axis. Only probes with hybridization intensities that plotted in the −149 to −20 region of PCA axis 1 (clustering of NA replicates) and in the 20 to 144 region of PCA axis 1 (clustering of SA replicates) were compiled, thereby excluding probes that plotted in the vector region (−20 to 20 of PCA axis 1) that did not contribute to clustering of samples. The hybridization intensities were averaged for each probe in replicate SA and NA arrays, and these values were used to calculate an intensity ratio between the SA and NA microbialite communities. A custom python script was used to bin each probe into a functional category. The average intensities for each probe for each functional category (e.g., stress response) were subjected to a Student's *t*-test to determine whether the differences in the intensity of hybridization of probes or suites of probes associated with replicate NA and SA samples were significantly different.

2.8 Microscopy

Hand samples were air-dried and examined using an edge digital microscope (Dino-light, CA). Images of SA and NA microbialite hand samples were taken between 20 and 200× magnification. High-resolution images of the SA and NA microbialites were taken using a Zeiss SUPRA 55VP field emission scanning electron microscope (FEM). FEM was carried out to perform a quantitative elemental analysis and to provide higher resolution analysis of the micromorphology of the SA and NA microbialites. Microbialite samples were air-dried prior to FEM analysis in order to facilitate elemental analysis. Sample preparation involved breaking the samples into smaller pieces which were adhered to the scanning puck using carbon tape. Samples were sputter-coated with platinum at 20 mA for 1 min and FEM images were taken using 5 kV for a better resolution while elemental analysis was performed at 20 kV. Images taken at 20 kV are a reference for elemental analysis.

2.9 X-Ray powder diffraction (XRD)

Bulk mineralogy was determined by XRD using a Scintagx1 diffraction system. Subsamples of SA and NA microbialites were sieved to <60 μm and ground using a mortar and pestle. Powder was placed on a slide with double-sided tape and subjected to continuous scanning at 0.020 degrees between 3 and 73 degrees Pheta at 2 degrees min^{-1}. An effort was made to detect clay minerals using USGS standard procedures (Poppe, Paskevich, Hathaway, & Blackwood, 2002). However, due to a lack of sample of suitable mass combined with low percentages of clays (<1–2 wt %), the results were inconclusive and thus are not shown.

3 Results

3.1 Microbialite structure

Microbialites from the SA and NA were classified within the non-laminated category and are of the littoral environment type where singular mounds prevail (Fig. 2A). Using Logan, Rezak, and Ginsburg's (1964) classification scheme, most samples reflect type-SH structures in a Mode V distribution (Logan, 1961) which would also fall under Carozzi's (1962) classification into zones three and four (Carozzi, 1962). These classifications describe structures that have a variable basal radius and that are stacked as successive cappings over preexisting irregularities (Logan, 1961), which are also described as composite rings and flat-topped mounds, or small isolated mounds (Carozzi, 1962). It was also observed that the SA microbialite structures included microbial mound rings devoid of material in the center, which are interpreted as erosional remnants of former microbialites (Fig. 2A) (Chidsey et al., 2015). The morphology of these samples is generally non-laminated, knobby, postular, with large pore spaces that are often cement filled (Figs 2B and 3) (Chidsey et al., 2015; Eardley, 1938; Halley, 1976). This type of texture is known as fenestral fabric where pores of ~1 to 5 mm diameter may be filled or partially filled by geopetal sediment and calcite or anhydrite (Shinn, 1983). Genesis of these types of pores occurs in modern intertidal or supratidal environments in marine systems (Shinn, 1983), which correspond with littoral or supralittoral environments in lakes.

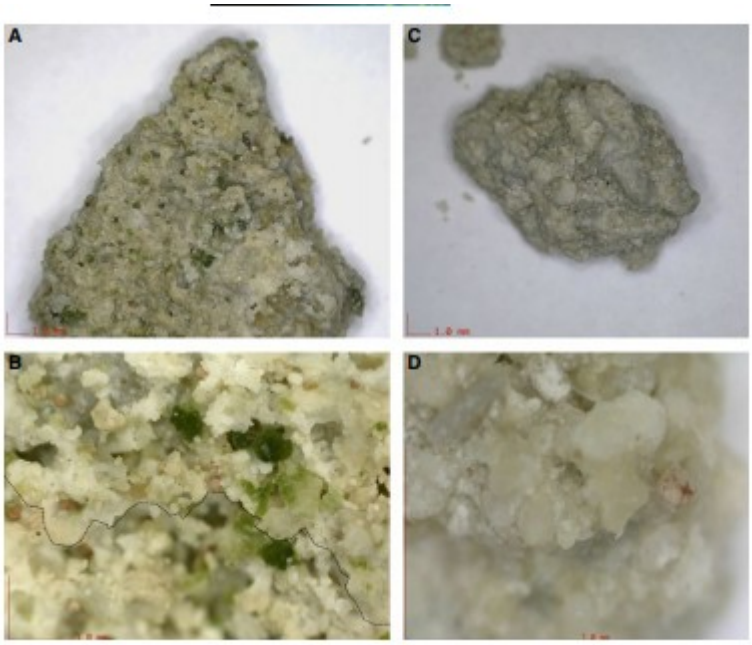

FIGURE 3 Dino-light images of South Arm (SA) and North Arm (NA) microbialite hand samples. A) SA magnification to 20×. B) SA magnification to 68× showing fenestral fabric and a major pore roughly 5 mm in diameter (out of focus and below black dotted line). C) NA magnification to 20×. D) NA magnification to 200×. Scale bars (1 mm) are indicated in each of the images

3.2 Microbialite mineralogy

Qualitative XRD analysis indicated that the most abundant mineral present in SA and NA microbialites is aragonite; other non-crystalline phases or minerals below the 1–2 wt % detection level are not seen in the bulk analysis and not reported (Fig. S1). FEM elemental spot and line analysis was then used to determine the mineralogy of the non-aragonite portion of each sample, which indicated the presence of quartz and clay in the NA (Fig. S3). Consistent with this observation, sand grains were observed in hand samples (Fig. S3). The aragonite crystals associated with the SA and NA reveal two types (Fig. 2C–F). Aragonite in the SA is characterized as smooth prismatic aragonite crystals overlain with micritic aragonite precipitates (Flügal, 2004; Tucker & Wright, 2008), while the aragonite in the NA is primarily characterized by smooth prismatic aragonite crystals without the micritic aragonite precipitates (Fig. 2C,D). Abiotic aragonite precipitation is hypothesized to form the smooth prismatic crystals (NA), while biotic aragonite precipitation forms the micritic aragonite (SA) (Pedone & Folk, 1996).

3.3 Microbialite community abundance

Quantitative PCR of archaeal and bacterial 16S rRNA genes and eukaryal 18S rRNA genes shows marked differences in the abundance of templates in SA microbialite when compared to the NA microbialite (Fig. 4). When combined, the total number of SSU rRNA gene templates from these three taxonomic domains was three orders of magnitude greater in the SA microbialite than

the NA microbialite ($4.3 \times 10^{11} \pm 1.55 \times 10^{10}$ and $1.2 \times 10^{8} \pm 3.7 \times 10^{7}$ gene templates gram dry mass^{-1}, respectively). The SA microbialites were dominated by bacterial 16S rRNA genes (80% of total templates), while the NA microbialites were dominated by eukaryal 18S rRNA genes (55% of total templates) (Fig. 4). Archaeal 16S rRNA gene templates were not abundant in either SA or NA microbialites (2.4% and 8.8% of total templates, respectively).

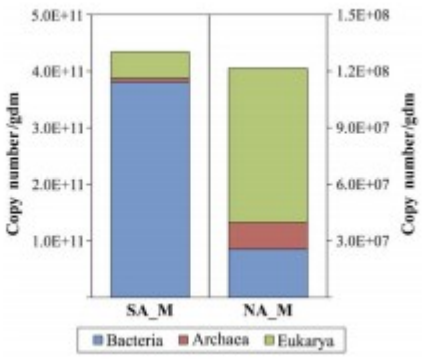

FIGURE 4 Abundances of archaeal, bacterial, and eukaryl small subunit (SSU) rRNA genes in South Arm (SA) and North Arm (NA) microbialites (M) as determined by quantitative PCR

3.4 Microbialite taxonomic diversity and composition—*Archaea*

A total of 5360 archaeal 16S rRNA gene sequences were sampled from SA and NA microbialites and adjacent planktonic communities, resulting in coverages of ~50% to 70% of the predicted diversity. The SA communities exhibited far greater species richness and diversity than the NA communities (Table 1). The SA microbialite and planktonic communities exhibited similar species richness and diversity. A comparison of the SA microbialite and adjacent planktonic communities indicated that they were more similar to each other (Bray–Curtis similarity = 0.48) than the NA microbialite and adjacent planktonic communities (Bray–Curtis similarity = 0.08) (Table 2).

TABLE 1 Predicted sequence coverage and inverse Simpson indices of archaeal, bacterial, and eukaryal small subunit (SSU) rRNA gene sequences recovered from South Arm (SA) and North Arm (NA) microbialite (M) and planktonic (P) communities

	Coverage	Inverse Simpson
Archaea		
SA_M	0.60	80.0
SA_P	0.68	49.1
NA_M	0.51	142
NA_P	0.73	14.7
Bacteria		
SA_M	0.76	14.6
SA_P	0.80	14.4
NA_M	0.83	24.2
NA_P	0.86	10.4
Eukarya		
SA_M	0.90	2.45
SA_P	0.87	3.86
NA_M	0.75	4.05
NA_P	0.86	2.92

TABLE 2 Bray–Curtis similarity indices of archaeal, bacterial, and eukaryal small subunit (SSU) rRNA genes recovered from South Arm (SA) and North Arm (NA) microbialite (M) and planktonic (P) communities. Bray–Curtis distances were calculated using the relative abundances of SSU rRNA gene OTUs as defined at 97% sequence similarity. Bold-faced values reflect comparisons between microbialite and planktonic communities for both SA and NA sampling locations

	SA_M	SA_P	NA_M	NA_P
Archaea				
SA_M	1.00	**0.48**	0.10	0.01
SA_P		1.00	0.10	0.01
NA_M			1.00	**0.08**
NA_P				1.00
Bacteria				
SA_M	1.00	**0.84**	0.51	0.50
SA_P		1.00	0.51	0.51
NA_M			1.00	**0.51**
NA_P				1.00
Eukarya				
SA_M	1.00	**0.73**	0.57	0.09
SA_P		1.00	0.11	0.13
NA_M			1.00	**0.40**
NA_P				1.00

The most abundant archaeal 16S rRNA gene OTU in the SA microbialite and planktonic communities (7.7% and 6.5% of total sequences,respectively) exhibited 100% sequence identity to *Halorubrum* sp. S26-1 within the order Haloferacales (Fig. 5A). The next most abundant OTU in the SA microbialite and planktonic communities (6.0% and 5.6% of total sequences, respectively) exhibited 95% sequence identity to Euryarchaeote J4.75-12, an unclassified organism previously detected in the hypersaline, stratified Solar Lake, Sinai, Egypt (Cytryn, Minz, Oremland, & Cohen, 2000).

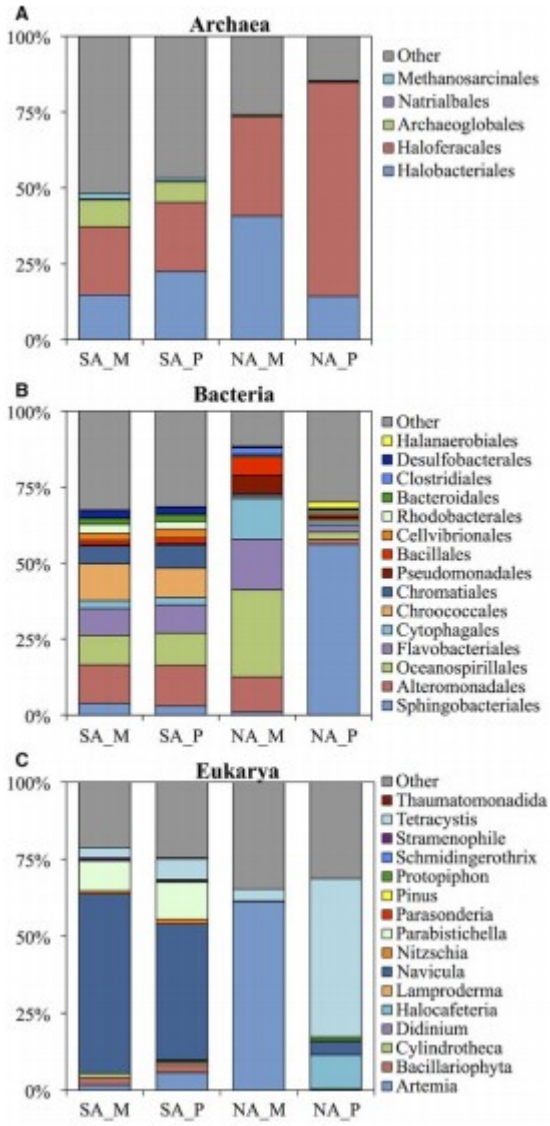

FIGURE 5 Composition of small subunit rRNA genes recovered from microbialite (M) and planktonic (P) communities in the South Arm (SA) and North Arm (NA). Representative OTUs for each library were binned at the order level for archaeal 16S rRNA genes (A), the order level for bacterial 16S rRNA genes (B), and the genus level for eukaryal 18S rRNA genes (C). Taxonomic bins at the same taxonomic level as indicated above that represented <1.0%, <1.0%, and <0.1% of the total sequences from each assemblage were pooled and depicted as “Other” for archaeal, bacterial, and eukaryal communities, respectively

The NA microbialite and planktonic 16S rRNA gene assemblages exhibited marked differences in their taxonomic composition and structure, and they were distinct from those sampled from the SA. The dominant OTU (6.0% of total sequences) recovered from the NA microbialite was closely related to *Halorubrum* sp. S26-1, the same dominant taxon identified in SA microbialites. The NA planktonic community was dominated (21.2% of total sequences) by an OTU with 97% sequence identity to *Halonotius pteroides* within the order Haloferacales. An OTU with 93% sequence identity to *Haloquadratum walsbyi* (Haloferacales), an extreme halophile with a

rectangular morphology, was also abundant in the NA planktonic community, accounting for 14.6% of the total recovered sequences (Fig. 5A).

3.4.1 Bacteria

A total of 5188 bacterial 16S rRNA gene sequences were sampled from SA and NA microbialite and adjacent planktonic communities, resulting in coverages of ~76% to 86% of the predicted diversity. The NA microbialite community exhibited greater species richness and diversity than the NA planktonic community, while the SA microbialite and planktonic communities exhibited similar species richness and diversity (Table 1). A comparison of the SA microbialite and adjacent planktonic communities indicated that they were more similar to each other (Bray–Curtis similarity = 0.84) than the NA microbialite and adjacent planktonic communities (Bray–Curtis similarity = 0.51) (Table 2).

The most abundant bacterial 16S rRNA gene OTU in SA microbialite and planktonic communities (12.7% and 13.4% of total sequences, respectively) exhibited 100% sequence identity to the heterotroph *Marinimicrobium haloxylanilyticum* within the order Alteromonadales. The next most abundant OTU in the SA microbialite and planktonic communities (12.0% and 9.6% of total sequences, respectively) exhibited 100% sequence identity to the halophilic cyanobacterium *Euhalothece* sp. MPI 96N304 within the order Chroococcales. The majority of additional bacterial OTUs associated with the SA microbialite and planktonic communities were closely affiliated with heterotrophic species, including the moderate halophile *Saccharospirillum salsuginis* within the order Oceanospirillales (Fig. 5B).

The NA microbialite and planktonic communities exhibited substantial differences in their taxonomic composition and structure, and they were distinct from those sampled from the SA. The dominant OTU (28.5% of total sequences) associated with the NA microbialite exhibited 94% sequence identity to the halophilic aerobe *Halomonas sediminis* within the order Oceanospirillales. An OTU with 100% sequence identity to *Pseudoalteromonas* sp. An100 within the order Altermonadales was also abundant in the NA microbialite, accounting for 11.5% of the total recovered sequences. The NA planktonic community was dominated (56% of total sequences) by an OTU with 100% sequence identity to the extreme halophile *Salinibacter ruber* within the order Sphingobacteriales (Fig. 5B).

3.4.2 Eukarya

A total of 1237 eukaryal 18S rRNA gene sequences were sampled from the microbialite and associated planktonic communities from the SA and NA, resulting in coverages of ~75% to 90% of the predicted diversity, respectively (Table 1). The NA microbialite community exhibited greater species richness and diversity than the SA microbialite community, while the SA planktonic community was more diverse than the NA planktonic community. The SA microbialite and associated planktonic communities were

more similar to each other (Bray–Curtis similarity = 0.73) than the NA microbialite and associated planktonic communities (Bray–Curtis similarity = 0.40) (Table 2).

The SA microbialite and planktonic communities were dominated (56% and 45% of total 18S rRNA gene sequences, respectively) by an OTU that was 98% identical to *Navicula salinicola*, a benthic diatom. Silica, a requirement for diatoms (Darley & Volcani, 1969), was detected by FEM in both SA and NA microbialites albeit at low levels (~ <4 wt %) (Fig. S2). This observation was further supported by microscopic analysis of microbialites which suggested the presence of sand grains (Fig. S3). Additional abundant OTUs associated with the SA microbialite and associated planktonic communities were closely affiliated with the green alga *Tetracystis texensis* (98% sequence identities) and the ciliate *Parabistichella variabilis* (99% sequence identities) (Fig. 5C).

The NA microbialite community was dominated (51% of total sequences) by two OTUs with close affiliation (99% and 98% identities) with the brine shrimp genus *Artemia*. This differed from the NA planktonic community, however, in that the most abundant (51% of total) sequence was most closely affiliated with the green alga *Tetracystis texensis,* which was only a minor component (4% of total) of the associated microbialite structure. Sequences affiliated with *Halocafeteria* sp., a bacterivorous nanoflagellate, were also identified in the water column of the NA (Fig. 5C). Unexpectedly, sequences with close affiliation to the brine fly genus *Ephedra* were not detected in either the NA or SA microbialite or planktonic communities.

3.5 Microbialite functional genomic variation

After quality filtering, a total of 46,155 probes corresponding to 939 unique genes were detected in genomic DNA extracted from SA and NA microbialites. Of these 939 unique genes, 882 were detected in both of the SA and NA microbialites, while only 31 and 26 genes were uniquely detected in SA and NA microbialites, respectively.

Principle component analysis ordination (Fig. 6) of the relative intensity of hybridization of SA and NA genomic DNA to these 46,155 probes revealed two clusters that separate primarily along coordinate 1 (37.1% of variance explained). Each of these clusters contained replicate DNA extracts from the SA or the NA microbialites. No clear pattern of clustering of samples was observed along PCA coordinate 2 (19.2% of variance explained). A total of 28,284 probes were identified that contributed to clustering along PCA coordinate 1. These probes were further filtered by taking the average ratio of their abundance when comparing the SA to the NA and vice versa. The probes which had an abundance of ≥0.2 fold were considered for further analysis. These probes were affiliated with 108 and 139 genes in the SA and NA microbialites, respectively (Tables S1–S3). The majority of these genes were involved in carbon cycling (13% and 16% in SA and NA microbialites, respectively), metal homeostasis (27% and 25% in SA and NA microbialites,

respectively), and response to stress (14% and 17% in SA and NA microbialites, respectively) (Fig. 7; Tables S1–S3). While the variation in the functional categories of probes detected in the SA and NA probes was similar, the differences in the average intensity of hybridization of probes (as demarcated by the aforementioned functional categories) were significantly different at $p < 0.05$ (Fig. 7; Tables S1–S3).

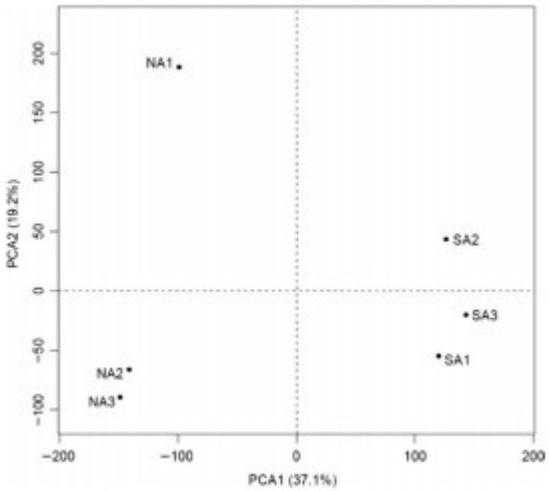

FIGURE 6 PCA ordination depicting the dissimilarity in the composition and intensity of GeoChip functional gene probes detected in triplicate South Arm (SA) and North Arm (NA) microbialite genomic DNA extracts. Additional details of genes identified in SA and NA microbialites and their hybridization intensity are presented in Tables S1–S3

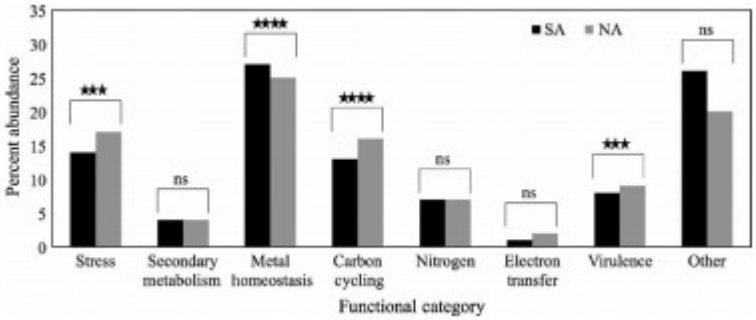

FIGURE 7 Ontology of genes, binned at the level of metabolic pathway, that exhibited different abundances based on probe hybridization intensity in South Arm (SA) and North Arm (NA) microbialite genomic DNA extracts. Only those probes that contributed to clustering based on PCA1 (37.1% of variation) and that had a signal intensity of ≥0.2 fold difference between the two samples were included in this analysis. Four stars: $p < 0.0001$; three stars: $p < 0.001$; two stars: $p < 0.01$, ns: not significant with a $p > 0.1$. Additional details of genes identified in SA and NA microbialites and their hybridization intensity are presented in Tables S1–S3

4 Discussion

In the present study, we exploited the presence of a railroad causeway constructed in 1959 at GSL and the salinity gradient that developed to characterize the similarities and differences associated with microbialites present in the less saline SA (12%–14%) and the more saline NA (24%–31%). The goal of this study was to identify the microbial populations that are most

likely involved in the formation of microbialite structures and to determine whether the NA microbialites are actively precipitating biogenic carbonate or if they are remnant features from prior to causeway construction. Of particular importance to our study is determining the relative abundance of phototrophic organisms in SA and NA microbialites, which are inferred to be the likely architects of microbialite structures in GSL (Wurtsbaugh et al., 2011) and elsewhere (Baumgartner et al., 2009; Pepe-Ranney et al., 2012; Riding, 2011).

Comparisons between the composition and abundance of archaeal, bacterial, and eukaryal 16S/18S rRNA gene assemblages in the SA and NA microbialite communities reveal distinct differences, in particular among OTUs inferred to be involved in photoautotrophy. The second most abundant bacterial 16S rRNA gene OTU (absolute abundance $4.6 \times 10^{10} \pm 1.7 \times 10^{10}$ templates gdm^{-1}) associated with the SA microbialite is closely affiliated with the halophilic cyanobacterium *Euhalothece* sp. MPI 96N304. The absence of *Euhalothece* in the NA is likely due to an inability to grow at salinities greater than 15% (Garcia-Pichel, Nubel, & Muyzer, 1998). In addition, the SA microbialite community harbored abundant sequences ($2.8 \times 10^{10} \pm 7.6 \times 10^{9}$ templates gdm^{-1}) closely affiliated with the photosynthetic diatom *Navicula*, which is also absent in the more saline NA. Like *Euhalothece*, the absence of sequences affiliated with *Navicula* in the NA is likely due to the inability of a number of strains within this genus to grow above ~21% salt (Javor, 1989). The only inferred photoautotroph identified in association with the NA microbialite is affiliated with the alga *Tetracystis* ($3.1 \times 10^{6} \pm 7.7 \times 10^{5}$ templates gdm^{-1}). Thus, the total abundance of 16S/18S rRNA gene templates associated with photoautotrophs in the SA microbialite is $7.4 \times 10^{10} \pm 1.6 \times 10^{10}$ templates gdm^{-1} and the NA microbialite is $3.3 \times 10^{6} \pm 7.8 \times 10^{5}$ templates gdm^{-1}. If these photoautotrophs are indeed the primary architects of SA GSL microbialite structures, then it is likely that the structures present in the NA of GSL are remnant and are not actively being formed, or are experiencing drastically lowered growth rates due to salinity constraints imposed on photoautotroph physiology (Joint et al., 2002).

The abundance of *Euhalothece* and *Navicula* associated with SA microbialites also implies that they provide photosynthate (e.g., polysaccharides) for abundant heterotrophs associated with SA microbialites, including an abundance of heterotrophs closely affiliated with the polysaccharide-degrading bacterium *Marinimicrobium haloxylanilyticum* (Møller, Kjeldsen, & Ingvorsen, 2010). Moreover, the presence of abundant photoautotrophs in the SA microbialite and their low abundance in the NA microbialite may help to explain the overall lower abundances of Archaea, Bacteria, and Eukarya in the latter, given that these communities are largely inferred to be heterotrophic and would therefore be dependent on allochthonous organic carbon sources. The difference in the abundance of microbial SSU rRNA gene templates (a proxy for biomass) in the SA and NA may also help to explain why the microbialite and planktonic microbial communities of the SA are

very similar to each other (Bray–Curtis Similarity = 0.48, 0.84, 0.73 for Archaea, Bacteria, and Eukarya), while this is not the case in the NA. More productive biofilm communities, as indicated by a higher amount of biomass (i.e., SA microbialite), are often associated with a greater extent of cell sloughing than less productive biofilm communities (i.e., NA microbialite) (Muffler & Ulber, 2014). If true, these sloughed cells would make it more difficult to detect or identify an endogenous planktonic community in the SA when compared to the NA.

The NA microbialite community was dominated by 18S rRNA genes closely affiliated with *Artemia* ($5.0 \times 10^7 \pm 1.2 \times 10^7$ templates gdm^{-1}), or brine shrimp, which were also in high abundance in the SA ($8.0 \times 10^8 \pm 2.2 \times 10^8$ templates gdm^{-1}). *Artemia* have previously been detected in waters with salinity measurements up to 34% and have seldom been detected in waters with salinity of less than 4.5%, which is likely due to the upper tolerance limit of their predators (Persoone & Sorgeloos, 1980). Brine shrimp have been shown to rely on algae as a primary food source and will also (secondarily) consume bacterial cells (Bond, 1933). One possible food source for *Artemia* is algae related to *Tetracystis,* which were dominant components of NA planktonic and microbialite communities while they only made up a small proportion of the SA planktonic and microbialite communities. The presence of another alga in the SA, the diatom *Navicula*, and the cyanobacterium *Euhalothece* may also serve as food sources for *Artemia*. Despite having available food sources in both the SA and the NA and being a large percentage of the biomass of the NA, *Artemia* 18S rRNA gene copies are still lower in the NA than the SA microbialites ($5.0 \times 10^7 \pm 1.2 \times 10^7$ and $8.0 \times 10^8 \pm 2.2 \times 10^8$ templates gdm^{-1}, respectively). This suggests that the low productivity of the NA microbialite community is less able to support large populations of heterotrophic eukaryotes than the more productive SA community. Interestingly, *Ephydra* spp. (brine flies) were not detected in any samples. One possible reason for this is that the *Ephydra* pupae may be too large to be aggregated in the microbialite concrete, while the much smaller *Artemia* cysts are readily aggregated and were observed in the microbialites in the present study (Figs 2E and 3).

The differences in microbialite communities sampled from the SA and NA were also apparent at the level of their functional gene composition. Consistent with SSU rRNA gene sequencing data which indicated the presence of abundant oxygenic phototrophs in the SA but not the NA is the detection of an abundance of genes in the SA microbialite involved in metal homeostasis (Fig. 7) including magnesium chelatase genes (Tables S1, S2). These genes, which were identified in the SA microbialite communities but not in the NA microbialite communities, encode for proteins involved in (bacterio)chlorophyll biosynthesis (Jaschke, Hardjasa, Digby, Hunter, & Beatty, 2011). Furthermore, genes encoding alkyl hyperoxide reductase, which functions to scavenge reactive oxygen compounds such as hydrogen peroxide (Jacobson, Morgan, Christman, & Ames, 1989), were found in high

abundance in SA microbialite communities when compared to the NA microbialite communities. Given that oxygenic photosynthesis often results in localized supersaturated O_2 conditions (Jensen, Steunou, Bhaya, Kühl, & Grossman, 2011), this result is also consistent with the prevalence of oxygenic phototrophs in the SA but not the NA microbialite communities.

Photoautotrophs often excrete organic molecules which help to sustain secondary heterotrophic consumers (Nold & Ward, 1996). As mentioned above, the abundance of 16S rRNA genes affiliated with inferred heterotrophs was higher in the SA microbialite ($3.6 \times 10^{11} \pm 1.6 \times 10^{11}$ templates gdm^{-1}) than the NA microbialite ($1.2 \times 10^{8} \pm 3.7 \times 10^{7}$ templates gdm^{-1}). Consistent with this observation, genes that enable use of complex organics such as cellulose (cellulose), hemicellulose (hemicellase), chitin (chitinase), and pectin (pectinase) were in higher abundance in the SA microbialite community when compared to the NA microbialite community (Tables S1–S3). In the case of the abundance of chitinase genes, this observation may reflect the higher abundance of brine shrimp and cysts in the SA microbialite, both of which contain chitin (Asadpour, Motallebi, & Eimanifar, 2007).

The SA microbialite community also showed a high abundance of an array of metal transporters that included genes encoding cobalt–zinc–cadmium resistance proteins, zinc uptake system proteins, magnesium transport proteins, and sodium and potassium transport proteins (Tables S1, S2). This could be due to the high levels of metals transported into GSL from industrial, urban, mining, and agricultural discharge into the SA through rivers that drain a 37,500-km^2 watershed that includes more than 1.7 million people and the Rio Tinto Kennecott Copper mine, among others (Naftz, Johnson, Freeman, Beisner, & Diez, 2008). Genes related to sodium/proton transport were detected in high abundance in NA (Tables S1, S3), which is consistent with the high salinity (24%–31%) associated with the NA and the stress that this imposes on microbial life (Oren, 2013). Genes encoding proteins involved in carotenoid biosynthesis such as beta-carotene dioxygenase were more abundant in NA microbialite communities than SA microbialite communities (Tables S1, S3). This is consistent with previous evidence indicating a propensity for halophiles, such as *Halobacterium, Halococcus, Haloarcula* among others, to synthesize large amounts of carotenoids (Yatsunami et al., 2014).

Molecular data compiled in this study indicate key differences in the taxonomic and functional composition of microbialite communities in the SA and NA and suggest that populations in the NA are likely colonizing remnant carbonate structures, while SA populations are likely involved in active carbonate precipitation. To further characterize this possibility, we examined the nature of aragonite precipitates on the surface of SA and NA microbialites. FEM imaging reveals both biotic and abiotic aragonite precipitation based on a previous characterization of aragonite cement in the SA of GSL (Pedone & Folk, 1996) (Fig. 2C–F). Smooth aragonite crystals,

which Pedone and Folk (1996) characterized as abiotic, are clearly seen in pore spaces in both the SA and NA microbialites, as indicated by arrows (Fig. 2C,D, respectively). However, micritic aragonite deposits (Flügal, 2004), interpreted to be biotic (Pedone & Folk, 1996), are only observed in the SA microbialite. This observation is consistent with active biotic precipitation of carbonate in the SA and primarily abiotic carbonate precipitation in the NA. Based on molecular data, the organisms likely to be responsible for biotic aragonite precipitation, at the time of sampling of microbialites characterized in the present study, are the photoautotrophs *Euhalothece* and *Navicula*, as these organisms consume CO_2 and are present only in the SA. Phototrophs in general are known to contribute micritic aragonite to microbialite structures (Flügal, 2004). Additional characterization of microbialites sampled from multiple locations is needed to confirm that these two phototrophs are the architects of GSL microbialites.

5 Conclusions

Moderately saline (11.8%), shallow near shore environments at GSL promote the activity of a limited diversity of cyanobacteria (*Euhalothece*) and diatoms (*Navicula*), which are hypothesized to be responsible for biotic aragonite precipitation and microbialite formation. The microbialites from GSL associated with these photoautotrophs are non-laminated, knobby, postular structures with large pore spaces that are often cement filled. These are classified as type-SH structures in a Mode V distribution (Logan, 1961) or as type three and four within the classification scheme of Carozzi (Carozzi, 1962). Fossilized microbialites with this classification include those present in the 1.1 Ga-year-old Missoula group (Horodyski, 1975) and those in 0.5 Ga Hoyt limestone (Logan et al., 1964). The characteristics shared between GSL microbialites and these ancient microbialites could possibly be attributed to the environment in which these structures form—littoral mudflats protected from wave action—or to the composition of the microbial mats that function as the architects of these structures (Logan, 1961). The GSL microbialites also share several similarities with modern stromatolites in Shark Bay, Australia (Flügal, 2004), including the presence of aragonite and a similar microbial community composition containing eukaryotic diatoms (Awramik & Riding, 1988; John, 1991). The stromatolites in Shark Bay have been compared to other ancient stromatolites forming in intertidal environments (Logan, 1961). These observations provide new insight into the identity of phototrophic populations likely involved in the formation of a specific microbialite morphology and thereby inform our understanding of the processes that may have been involved in the formation of similar structures present in the geologic record (Allwood et al., 2006; Bosak et al., 2013; Sugitani et al., 2015; Van Kranendonk et al., 2008).

Photoautotrophs typically form the base of food chains and thus directly modulate biomass production (Wurtsbaugh et al., 2011). The detection of abundant photoautotrophs in the SA and their near complete absence in the NA suggests that the construction of the railroad causeway and the

subsequent increase in salinity has substantially altered the ecology of the NA and has likely had an impact on the productivity of this portion of the lake. Moreover, it has likely resulted in the demise of biogenic microbialite formation in the NA through inhibition of the primary architects of GSL microbialites, halophilic cyanobacteria and diatoms (Wurtsbaugh et al., 2011), which then limits the amount of food (e.g., brine shrimp) available to higher trophic levels including migrating birds. The detection of putatively biogenic micritic aragonite in the SA and its absence in the NA is consistent with this conclusion.

GSL microbialites share similar morphology with fossilized microbialites in the geological record. This similar morphology may result from similar environmental settings during their formation (i.e., moderate salinity, littoral environments protected from wave action), similar microbial populations involved in their formation (i.e., halophilic cyanobacteria, diatoms), or a combination of these factors. Considering that NA microbialite communities are no longer significantly precipitating carbonate despite being located in littoral environments (that prior to causeway construction originally promoted their formation) alludes to the central role of specific microbial populations and their activities in the formation of this microbialite morphology.

Acknowledgments

The authors thank Laura Kellerman for her assistance and expertise with the field emission scanning electron microscope, Dr. Karlene Hoo, Dean of the Montana State University Graduate School, for providing funds to help defray costs associated with our Precambrian Biosphere graduate class project, Dr. Mark Jutila for providing funds that enabled a class field trip to the Bridger Mountains to observe a stromatolite fossil bed, Donald L. Clark from the Utah Geologic Survey for careful review of this manuscript, and Charles G. Oviatt for helpful discussions regarding the geologic history of GSL. This work was supported by a grant from the Utah Department of Natural Resources Division of Forestry, Fire & State Lands (BKB and ESB) and a grant (NNA15BB02A) from the NASA Astrobiology Institute (JRS and ESB).

References

Allwood, A. C., Walter, M. R., Kamber, B. S., Marshall, C. P., & Burch, I. W. (2006). Stromatolite reef from the Early Archaean era of Australia. *Nature*, 441, 714– 718.

Anderson, R. B., Naftz, D. L., Day-Lewis, F. D., Henderson, R. D., Rosenberry, D. O., Stolp, B. J., & Jewell, P. (2014). Quantity and quality of groundwater discharge in a hypersaline lake environment. *Journal of Hydrology*, 512, 177–194.

Asadpour, Y., Motallebi, A., & Eimanifar, A. (2007). Biotechnological approach to produce chitin and chitosan from the shells of *Artemia urmiana* Günther,

1899 (Branchiopoda, Anostraca) Cysts from Urmia Lake, Iran. *Crustaceana*, 80, 171– 180.

Awramik, S. M., & Riding, R. (1988). Role of algal eukaryotes in subtidal columnar stromatolite formation. *Proceedings of the National Academy of Sciences of the USA*, 85, 1327– 1329.

Baskin, R. L. (2014). *Occurrence and spatial distribution of microbial bioherms in Great Salt Lake* (p. 203). Utah: The University of Utah.

Baskin, R. L., & Allen, D. V. (2005). *Bathymetric map of the south part of Great Salt Lake*. Utah: US Geological Survey.

Baskin, R. L., Driscoll, N. W., & Wright, V. P. (2013). Controls on lacustrine microbialite distribution in Great Salt Lake, Utah. In: B. Vining, K. Gibbons, W. Morgan, D. Bosence, D. Le Heron, E. Le Ber & T. Pritchard (Eds.), *Microbial carbonates in space and time: implications for global exploration and production*. Programme and Abstract Volume (pp. 70– 71). London: Geological society of London.

Baskin, R. L., & Turner, J. (2006). *Bathymetric map of the north part of Great Salt Lake*. Utah: US Geological Survey.

Baskin, R., Wright, V., Driscoll, N., Kent, G., & Hepner, C. (2012). Microbialite bioherms in Great Salt Lake, Utah: Influence of active tectonics and anthropogenic effects. In: *American Association of Petroleum Geologists Hedburg Conference*, Houston, TX.

Baumgartner, L. K., Dupraz, C., Buckley, D. H., Spear, J. R., Pace, N. R., & Visscher, P. T. (2009). Microbial species richness and metabolic activities in hypersaline microbial mats: Insight into biosignature formation through lithification. *Astrobiology*, 9, 861– 874.

Baxter, B. K., Litchfield, C. D., Sowers, K., Griffith, J. D., Dassarma, P. A., & Dassarma, S. (2005). Microbial diversity of Great Salt Lake. In N. Gunde-Cimerman, A. Oren & A. Plemenitaš (Eds.), *Adaptation to life at high salt concentrations in Archaea, Bacteria, and Eukarya* (pp. 9– 25). Dordrecht, the Netherlands: Springer.

Bond, R. (1933). Observations on *Artemia* “franciscana” Kellogg, especially on the relation of environment to morphology. *Internationale Revue der gesamten Hydrobiologie und Hydrographie*, 28, 117– 125.

Bosak, T., Knoll, A. H., & Petroff, A. P. (2013). The meaning of stromatolites. *Annual Review Earth and Planetary Science*, 41, 21– 44.

Bouton, A., Vennin, E., Boulle, J., Pace, A., Bourillot, R., Thomazo, C., … Visscher, P. T. (2016). Linking the distribution of microbial deposits from the Great Salt Lake (Utah, USA) to tectonic and climatic processes. *Biogeosciences Discussions*.

Boyd, E. S., Hamilton, T. L., Swanson, K. D., Howells, A. E., Baxter, B. K., Meuser, J. E., … Peters, J. W. (2014). [FeFe]-hydrogenase abundance and

diversity along a vertical redox gradient in Great Salt Lake, USA. *International Journal of Molecular Science*, 15, 21947– 21966.

Braithwaite, C. J. R., & Zedef, V. (1994). Living hydromagnesite stromatolites from Turkey. *Sedimentary Geology*, 92, 1– 5.

Cannon, J. S., & Cannon, M. A. (2002). The Southern Pacific railroad trestle – past and present. In J. W. Gwynn (Ed.), *Great Salt Lake, an overview of change*. Salt Lake City, UT: Special Publication of the Utah Department of Natural Resources.

Carozzi, A. V. (1962). Observations on algal biostromes in the Great Salt Lake, Utah. *Journal of Geology*, 70, 246– 252.

Chidsey, T. C. Jr, Vanden Berg, M. D., & Eby, D. E. (2015). Petrography and characterization of microbial carbonates and associated facies from modern Great Salt Lake and Uinta Basin's Eocene Green River Formation in Utah, USA. *Microbial Carbonates in Space and Time: Implications for Global Exploration and Production*, 418, 261– 286.

Cohen, A. S., Talbot, M. R., Awramik, S. M., Dettman, D. L., & Abell, P. (1997). Lake level and paleoenvironmental history of Lake Tanganyika, Africa, as inferred from late Holocene and modern stromatolites. *Geological Society of America Bulletin*, 109, 444– 460.

Cohenour, R., & Thompson, K. (1966). Geologic setting of Great Salt Lake. In J. K. Rigby (Ed.), *Guidebook to the Geology of Utah* (pp. 35– 56). Salt Lake City , UT: Utah Geological Society.

Collins, N. (1980). Population ecology of *Ephydra cinerea* Jones (Diptera: Ephydridae), the only benthic metazoan of the Great Salt Lake, USA. *Hydrobiologia*, 68, 99– 112.

Collins, L., & Jahnert, R. (2014). Stromatolite research in the Shark Bay World Heritage Area. *Royal Society of Western Australia*, 97, 189– 219.

Colman, S. M., Kelts, K. R., & Dinter, D. A. (2002). Depositional history and neotectonics in Great Salt Lake, Utah, from high-resolution seismic stratigraphy. *Sedimentary Geology*, 148, 61– 78.

Cytryn, E., Minz, D., Oremland, R. S., & Cohen, Y. (2000). Distribution and diversity of archaea corresponding to the limnological cycle of a hypersaline stratified lake (Solar Lake, Sinai, Egypt). *Applied and Environmental Microbiology*, 66, 3269– 3276.

Darley, W. M., & Volcani, B. E. (1969). Role of silicon in diatom metabolism: A silicon requirement for deoxyribonucleic acid synthesis in the diatom *Cylindrotheca fusiformis* Reimann and Lewin. *Experimental Cell Research*, 58, 334– 342.

Domagalski, J. L., Orem, W. H., & Eugster, H. P. (1989). Organic geochemistry and brine composition in Great Salt, Mono, and Walker Lakes. *Geochimica Et Cosmochimica Acta*, 53, 2857– 2872.

Dowd, S. E., Sun, Y., Secor, P. R., Rhoads, D. D., Wolcott, B. M., James, G. A., & Wolcott, R. D. (2008). Survey of bacterial diversity in chronic wounds using pyrosequencing, DGGE, and full ribosome shotgun sequencing. *BMC Microbiology*, 8, 1– 15.

Dupraz, C., Reid, R. P., Braissant, O., Decho, A. W., Norman, R. S., & Visscher, P. T. (2009). Processes of carbonate precipitation in modern microbial mats. *Earth-Science Reviews*, 96, 141– 162.

Dupraz, C., & Visscher, P. T. (2005). Microbial lithification in marine stromatolites and hypersaline mats. *Trends in Microbiology*, 13, 429– 438.

Eardley, A. J. (1938). Sediments of Great Salt Lake, Utah. *AAPG Bulletin*, 22, 1305– 1411.

Edgar, R. C., Haas, B. J., Clemente, J. C., Quince, C., & Knight, R. (2011). UCHIME improves sensitivity and speed of chimera detection. *Bioinformatics*, 27, 2194– 2200.

Edgcomb, V. P., Bernhard, J. M., Summons, R. E., Orsi, W., Beaudoin, D., & Visscher, P. T. (2014). Active eukaryotes in microbialites from Highborne Cay, Bahamas, and Hamelin Pool (Shark Bay), Australia. *The ISME Journal*, 8, 418– 429.

Flügal, E. (2004). *Microfaces of carbonate rocks: Analysis, interpretation, and application*. Germany: Springer.

Foster, J. S., & Green, S. J. (2011) Microbial diversity in modern stromatolites. In V. C. Tewari & J. Seckbach (Eds.), *Stromatolites: Interaction of microbes with sediments* (pp. 383– 405). Berlin, Germany: Springer.

Garcia-Pichel, F., Nubel, U., & Muyzer, G. (1998). The phylogeny of unicellular, extremely halotolerant cyanobacteria. *Archives of Microbiology*, 169, 469– 482.

Gebelein, C. D. (1969). Distribution, morphology, and accretion rate of recent subtidal algal stromatolites, Bermuda. *Journal of Sedimentary Petrology*, 39, 49– 69.

Gerard, E., Menez, B., Couradeau, E., Moreira, D., Benzerara, K., Tavera, R., & Lopez-Garcia, P. (2013). Specific carbonate-microbe interactions in the modern microbialites of Lake Alchichica (Mexico). *The ISME Journal*, 7, 1997– 2009.

Greer, D. C. (1971). Annals map supplement fourteen: Great Salt Lake, Utah. *Annals of the Association of American Geographers*, 61, 214– 215.

Gwynn, J. W. (1996). *Commonly asked questions about Utah's Great Salt Lake and Ancient Lake Bonneville*. Salt Lake City, UT: Utah Geological Survey.

Halley, R. B. (1976). Textural variation within Great Salt Lake algal mounds. *Developments in Sedimentology*, 20, 435– 445.

Hamilton, T. L., Peters, J. W., Skidmore, M. L., & Boyd, E. S. (2013). Molecular evidence for an active endogenous microbiome beneath glacial ice. *The ISME Journal*, 7, 1402– 1412.

Hassibe, W. R., & Keck, W. G. (1991). *The Great Salt Lake*. Reston, VA: US Geological Survey.

Horodyski, R. J. (1975). Stromatolites of the lower Missoula Group (Middle Proterozoic), Belt Supergroup, Glacier National Park, Montana. *Precambrian Research*, 2, 215– 254.

Jacobson, F. S., Morgan, R. W., Christman, M. F., & Ames, B. N. (1989). An alkyl hydroperoxide reductase from *Salmonella typhimurium* involved in the defense of DNA against oxidative damage - Purification and properties. *Journal of Biological Chemistry*, 264, 1488– 1496.

Jahnert, R. J., & Collins, L. B. (2011). Significance of subtidal microbial deposits in Shark Bay, Australia. *Marine Geology*, 286, 106– 111.

Jaschke, P. R., Hardjasa, A., Digby, E. L., Hunter, C. N., & Beatty, J. T. (2011). A *bchD* (magnesium chelatase) mutant of *Rhodobacter sphaeroides* synthesizes zinc bacteriochlorophyll through novel zinc-containing intermediates. *Journal of Biological Chemistry*, 286, 20313– 20322.

Javor, B. (1989). *Hypersaline environments: Microbiology and biogeochemistry*. Berlin: Springer-Verlag.

Jensen, S. I., Steunou, A.-S., Bhaya, D., Kühl, M., & Grossman, A. R. (2011). *In situ* dynamics of O_2, pH and cyanobacterial transcripts associated with CCM, photosynthesis and detoxification of ROS. *The ISME Journal*, 5, 317– 328.

John, J. (1991). *Climaconeis stromatolitis*, a new species of diatom from Shark Bay, Western Australia. *Diatom Research*, 6, 49– 54.

Joint, I., Henriksen, P., Garde, K., & Riemann, B. (2002). Primary production, nutrient assimilation and microzooplankton grazing along a hypersaline gradient. *FEMS Microbial Ecology*, 39, 245– 257.

Jones, B. F., Naftz, D. L., Spencer, R. J., & Oviatt, C. G. (2009). Geochemical evolution of Great Salt Lake, Utah, USA. *Aquatic Geochemistry*, 15, 95– 121.

Laval, B., Cady, S. L., Pollack, J. C., Mckay, C. P., Bird, J. S., Grotzinger, J. P., ... Bohm, H. R. (2000). Modern freshwater microbialite analogues for ancient dendritic reef structures. *Nature*, 407, 626– 629.

Le, S., Josse, J., & Husson, F. (2008). FactoMineR: An R package for multivariate analysis. *Journal of Statistical Software*, 25, 1– 18.

Liang, Y., He, Z., Wu, L., Deng, Y., Li, G., & Zhou, J. (2010). Development of a common oligonucleotide reference standard for microarray data normalization and comparison across different microbial communities. *Applied and Environmental Microbiology*, 76, 1088– 1094.

Logan, B. W. (1961). Cryptozoon and associate stromatolites from the recent, Shark Bay, Western-Australia. *The Journal of Geology*, 69, 517.

Logan, B. W., Rezak, R., & Ginsburg, R. N. (1964). Classification and environmental significance of algal stromatolites. *The Journal of Geology*, 72, 68– 83.

Meuser, J. E., Baxter, B. K., Spear, J. R., Peters, J. W., Posewitz, M. C., & Boyd, E. S. (2013). Contrasting patterns of community assembly in the stratified water column of Great Salt Lake, Utah. *Microbial Ecology*, 66, 268– 280.

Mohapatra, G. K., & Johnson, R. A. (1998). Localization of listric faults at thrust fault ramps beneath the Great Salt Lake Basin, Utah: Evidence from seismic imaging and finite element modeling. *Journal of Geophysical Research: Solid Earth*, 103, 10047– 10063.

Møller, M. F., Kjeldsen, K. U., & Ingvorsen, K. (2010). *Marinimicrobium haloxylanilyticum* sp. nov., a new moderately halophilic, polysaccharide-degrading bacterium isolated from Great Salt Lake, Utah. *Antonie Van Leeuwenhoek*, 98, 553– 565.

Muffler, K., & Ulber, R. (2014). *Productive Biofilms*. Berlin: Springer-Verlag.

Myshrall, K. L., Mobberley, J. M., Green, S. J., Visscher, P. T., Havemann, S. A., Reid, R. P., & Foster, J. S. (2010). Biogeochemical cycling and microbial diversity in the thrombolitic microbialites of Highborne Cay, Bahamas. *Geobiology*, 8, 337– 354.

Naftz, D. L., Johnson, W. P., Freeman, M., Beisner, K., & Diez, X. (2008). *Estimation of selenium loads entering the south arm of Great Salt Lake, Utah* (pp. 1– 50). Reston, VA: US Geological Survey.

Naftz, D. L., Millero, F. J., Jones, B. F., & Green, W. R. (2011). An equation of state for hypersaline water in Great Salt Lake, Utah, USA. *Aquatic Geochemistry*, 17, 809– 820.

Noffke, N., & Awramik, S. (2013). Stromatolites and MISS—differences between relatives. *GSA Today*, 23, 4– 9.

Nold, S. C., & Ward, D. M. (1996). Photosynthate partitioning and fermentation in hot spring microbial mat communities. *Applied and Environmental Microbiology*, 62, 4598– 4607.

Oren, A. (2013). Life at high salt concentrations. In E. Rosenberg, E. F. Delong, S. Lory, E. Stackebrandt, & F. Thompson (Eds.), *The prokaryotes: Prokaryotic communities and ecophysiology* (pp. 421– 440). Heidelberg, Berlin: Springer.

Osborne, R. H., Licari, G. R., & Link, M. H. (1982). Modern lacustrine stromatolites, Walker Lake, Nevada. *Sedimentary Geology*, 32, 39– 61.

Oviatt, C. G., Madsen, D. B., Miller, D. M., Thompson, R. S., & Mcgeehin, J. P. (2015). Early Holocene Great Salt Lake, USA. *Quaternary Research*, 84, 57– 68.

Oviatt, C. G., Thompson, R. S., Kaufman, D. S., Bright, J., & Forester, R. M. (1999). Reinterpretation of the Burmester Core, Bonneville Basin, Utah. *Quaternary Research*, 52, 180– 184.

Pages, A., Welsh, D. T., Teasdale, P. R., Grice, K., Vacher, M., Bennett, W. W., & Visscher, P. T. (2014). Diel fluctuations in solute distributions and biogeochemical cycling in a hypersaline microbial mat from Shark Bay, WA. *Marine Chemistry*, 167, 102– 112.

Parnell, J. J., Rompato, G., Latta, L. C. I. V., Pfrender, M. E., Van Nostrand, J. D., He, Z., … Weimer, B. C. (2010). Functional biogeography as evidence of gene transfer in hypersaline microbial communities. *PLoS ONE*, 5, e12919.

Pedone, V. A., & Folk, R. L. (1996). Formation of aragonite cement by nannobacteria in the Great Salt Lake, Utah. *Geology*, 24, 763– 765.

Pepe-Ranney, C., Berelson, W. M., Corsetti, F. A., Treants, M., & Spear, J. R. (2012). Cyanobacterial construction of hot spring siliceous stromatolites in Yellowstone National Park. *Environmental Microbiology*, 14, 1182– 1197.

Persoone, G., & Sorgeloos, P (1980) General aspects of the ecology and biogeography of *Artemia*. In G. Persoone, P. Sorgeloos, O. Roels & E. Jaspers (Eds.), *The brine shrimp Artemia* (pp. 456)., Wetteren, Belgium: Universa Press.

Poppe, L. J., Paskevich, V. F., Hathaway, J. C., & Blackwood, D. S. (2002). *A laboratory manual for X-ray powder diffraction*. Reston, VA, USA: US Geological Survey.

Post, F. J. (1977). Microbial ecology of Great Salt Lake. *Microbial Ecology*, 3, 143– 165.

Reid, R. P., Visscher, P. T., Decho, A. W., Stolz, J. F., Bebout, B. M., Dupraz, C., … Desmarais, D. J. (2000). The role of microbes in accretion, lamination and early lithification of modern marine stromatolites. *Nature*, 406, 989– 992.

Riding, R. (2000). Microbial carbonates: The geological record of calcified bacterial-algal mats and biofilms. *Sedimentology*, 47, 179– 214.

Riding, R. (2011) Microbialites, stromatolites, and thrombolites. In J. Reitner & V. Thiel (Eds.), *Encyclopedia of Geobiology* (pp. 635– 654). Dordrecht, the Netherlands: Springer.

Roney, H. C., Booth, G. M., & Cox, P. A. (2009). Competitive exclusion of Cyanobacterial species in the Great Salt Lake. *Extremophiles*, 13, 355– 361.

Schloss, P. D., Westcott, S. L., Ryabin, T., Hall, J. R., Hartmann, M., Hollister, E. B., … Weber, C. F. (2009). Introducing mothur: Open-source, platform-independent, community-supported software for describing and comparing

microbial communities. *Applied and Environmental Microbiology*, 75, 7537–7541.

Sei, A., & Fathepure, B. Z. (2009). Biodegradation of BTEX at high salinity by an enrichment culture from hypersaline sediments of Rozel Point at Great Salt Lake. *Journal of Applied Microbiology*, 107, 2001– 2008.

Shinn, E. A. (1983). Birdseyes, fenestrae, shrinkage pores, and loferites - A reevaluation. *Journal of Sedimentary Petrology*, 53, 619– 628.

Souza, V., Espinosa-Asuar, L., Escalante, A. E., Eguiarte, L. E., Farmer, J., Forney, L., … Elser, J. J. (2006). An endangered oasis of aquatic microbial biodiversity in the Chihuahuan desert. *Proceedings of the National Academy of Sciences of the USA*, 103, 6565– 6570.

Sugitani, K., Mimura, K., Takeuchi, M., Lepot, K., Ito, S., & Javaux, E. (2015). Early evolution of large micro-organisms with cytological complexity revealed by microanalyses of 3.4 Ga organic-walled microfossils. *Geobiology*, 13, 507– 521.

Tazi, L., Breakwell, D. P., Harker, A. R., & Crandall, K. A. (2014). Life in extreme environments: Microbial diversity in Great Salt Lake, Utah. *Extremophiles*, 18, 525– 535.

Tucker, M. E., & Wright, V. (2008). *Carbonate sedimentology*, Malden, MA: Blackwell Science.

Van Kranendonk, M. J., Philippot, P., Lepot, K., Bodorkos, S., & Pirajno, F. (2008). Geological setting of Earth's oldest fossils in the ca. 3.5 Ga Dresser Formation, Pilbara Craton, Western Australia. *Precambrian Research*, 167, 93– 124.

Vanden Berg, M. D., Chidsey, T. C., Jr., Eby, D. E., & Kelln, W. (2015). Characterization of Microbialites in Bridger Bay, Antelope Island, Great Salt Lake, Utah. *6th International Limnogeology Congress*.

Velasco, M. S., Bennett, R. A., Johnson, R. A., & Hreinsdóttir, S. (2010). Subsurface fault geometries and crustal extension in the eastern Basin and Range Province, western U.S. *Tectonophysics*, 488, 131– 142.

Walter, M. R., Buick, R., & Dunlop, J. S. R. (1980). Stromatolites 3400–3500 Myr old from the North Pole area, Western Australia. *Nature*, 284, 443– 445.

Wang, Q., Garrity, G. M., Tiedje, J. M., & Cole, J. R. (2007). Naive Bayesian classifier for rapid assignment of rRNA sequences into the new bacterial taxonomy. *Applied and Environmental Microbiology*, 73, 5261– 5267.

Wang, C., Wang, X., Liu, D., Wu, H., Lü, X., Fang, Y., … Bai, E. (2014). Aridity threshold in controlling ecosystem nitrogen cycling in arid and semi-arid grasslands. *Nature Communications*, 5, 1– 8.

Wurtsbaugh, W. A. (2009). Biostromes, brine flies, birds and the bioaccumulation of selenium in Great Salt Lake, Utah. *Natural Resources & Environment*, 15, 2.

Wurtsbaugh, W. A., Gardberg, J., & Izdepski, C. (2011). Biostrome communities and mercury and selenium bioaccumulation in the Great Salt Lake (Utah, USA). *Science of the Total Environment*, 409, 4425– 4434.

Yatsunami, R., Ando, A., Yang, Y., Takaichi, S., Kohno, M., Matsumura, Y., ... Nakamura, S. (2014). Identification of carotenoids from the extremely halophilic archaeon *Haloarcula japonica*. *Frontiers in Microbiology*, 5, 1– 5.